

Article

Development of Hydrogen-Bonded Dimer-Type Photoluminescent Liquid Crystals of Fluorinated Tolane-carboxylic Acid

Shigeyuki Yamada ^{1,*}, Mitsuki Kataoka ^{1,†}, Keigo Yoshida ^{1,†}, Masakazu Nagata ^{2,‡}, Tomohiro Agou ², Hiroki Fukumoto ² and Tsutomu Konno ¹

¹ Faculty of Molecular Chemistry and Engineering, Kyoto Institute of Technology, Matsugasaki, Sakyo-ku, Kyoto 606-8585, Japan

² Department of Quantum Beam Science, Graduate School of Science and Engineering, Ibaraki University, 4-12-1 Nakanarusawa, Hitachi 316-8511, Ibaraki, Japan

* Correspondence: syamada@kit.ac.jp; Tel.: +81-75-724-7517

† The authors contributed equally to this work.

‡ Current address: Organic Materials Chemistry Group, Sagami Chemical Research Institute, Hayakawa 2743-1, Ayase 252-1193, Kanagawa, Japan.

Abstract: Functional molecules possessing photoluminescence (PL) and liquid-crystalline (LC) behaviors, known as photoluminescent liquid crystals, along with a small molecular structure, have attracted significant attention. Fluorinated tolane skeletons are small π -conjugated structures, which are promising candidates for such functional molecules. These structures were revealed to exhibit strong PL in solid state but no LC behavior. Based on a report on hydrogen-bonded dimer-type LC molecules of carboxylic acid, in this study, we designed and synthesized a series of fluorinated tolane-carboxylic acids (2,3,5,6-tetrafluoro-4-[2-(4-alkoxyphenyl)ethyn-1-yl]benzoic acids) as promising PLLC molecules. Evaluation of the LC behavior revealed that fluorinated tolane-carboxylic acids with a longer alkoxy chain than a butoxy chain exhibited nematic LC behavior. Additionally, fluorinated tolane-carboxylic acids showed intense PL in the solution and crystalline states. Notably, fluorinated tolane-carboxylic acid with an aggregated structure in the nematic LC phase also exhibited PL with a slight blue shift in PL maximum wavelength compared to the crystalline state. The present fluorinated tolane-carboxylic acid exhibiting PL and LC characteristics in a single molecule can be applied to thermoresponsive PL materials, such as a PL thermosensor.

Keywords: diphenylacetylene; fluorinated tolane-carboxylic acid; fluorine; photoluminescence; liquid crystals; nematic phase; phase transition



Citation: Yamada, S.; Kataoka, M.; Yoshida, K.; Nagata, M.; Agou, T.; Fukumoto, H.; Konno, T. Development of Hydrogen-Bonded Dimer-Type Photoluminescent Liquid Crystals of Fluorinated Tolane-carboxylic Acid. *Crystals* **2023**, *13*, 25. <https://doi.org/10.3390/cryst13010025>

Academic Editors: Ingo Dierking, Charles Rosenblatt, Kyosuke Isoda, Takahiro Ichikawa, Kosuke Kaneko, Mizuho Kondo, Tsuneaki Sakurai, Atsushi Seki, Mitsuo Hara and Go Watanabe

Received: 24 November 2022

Revised: 19 December 2022

Accepted: 21 December 2022

Published: 23 December 2022



Copyright: © 2022 by the authors. Licensee MDPI, Basel, Switzerland. This article is an open access article distributed under the terms and conditions of the Creative Commons Attribution (CC BY) license (<https://creativecommons.org/licenses/by/4.0/>).

1. Introduction

Photoluminescent liquid crystals, which possess photoluminescence (PL) and liquid-crystalline (LC) characteristics in a single molecule, have gained recognition as essential organic functional molecules owing to their extensive applicability in PL thermometers and thermoresponsive PL sensors [1–3]. To date, many PLLC molecules have been developed [4,5], which consist of large molecular structures with a π -conjugated structure, mesogenic core, and flexible unit that result in PL and LC behaviors. Therefore, developing PLLC molecules with a small molecular structure is necessary for practical applications considering the manufacturing costs and processes. An effective approach to searching for PLLC molecules with a small molecular structure is designing a common π -conjugated structure that functions as the core structure of PL and LC molecules.

Over the past few years, our group has focused on developing fluorine-containing organic functional molecules with a PL and an LC characteristic [6–14]. Our recent study revealed that fluorinated bistolane-based PLLC molecules (**A**) exhibit PL and LC behaviors

2. Materials and Methods

2.1. General

Column chromatography was performed for purification using Wakogel® 60N (38–100 μm), and thin layer chromatography (TLC) analysis was performed on silica gel TLC plates (silica gel 60F₂₅₄, Merck). The melting temperature (T_m) and clearing temperature (T_c) were determined using polarized optical microscopy (POM). ¹H and ¹³C nuclear magnetic resonance (NMR) spectra were obtained using a Bruker AVANCE III 400 NMR spectrometer (¹H: 400 MHz and ¹³C: 100 MHz) in chloroform-*d* (CDCl₃) or dimethyl sulfoxide-*d*₆ or acetone-*d*₆, and chemical shifts were reported in parts per million (ppm) using the residual proton in the NMR solvent. ¹⁹F NMR (376 MHz) spectra were obtained using a Bruker AVANCE III 400 NMR spectrometer in CDCl₃; CFCl₃ ($\delta_F = 0.0$ ppm) and hexafluorobenzene ($\delta_F = -163$ ppm) were used as internal standards. Infrared (IR) spectra were recorded using the KBr method with a JASCO FT/IR-4100 type A spectrometer; all spectra were reported in wavenumber (cm⁻¹) unit. High-resolution mass spectrometry (HRMS) was performed on a JEOL JMS-700MS spectrometer using the fast atom bombardment (FAB) method. Synthetic precursor ethyl 4-[2-(4-alkoxyphenyl)ethyn-1-yl]-2,3,5,6-tetrafluorobenzoate (**2**) was stated in a previous study and synthesized according to the reported procedure [12].

2.2. Typical Synthetic Procedure of 2,3,5,6-Tetrafluoro-2-[4-(methoxyphenyl)ethyn-1-yl]benzoic acid (**1a**)

Ethyl 2,3,5,6-tetrafluoro-4-[2-(4-methoxyphenyl)ethyn-1-yl]benzoate (**2a**, 2.0 g, 5.7 mmol), tetrahydrofuran (THF, 28 mL), and H₂O (12 mL) were placed in a two-necked round-bottomed flask, followed by addition of LiOH·H₂O (0.6 g, 14 mmol). The mixture was stirred at room temperature for 20 h and then acidified by adding an aqueous solution of HCl until the pH of the solution was below 1. The crude product was extracted with Et₂O (10 mL, three times), while the organic layer was washed with brine (20 mL, once). The collected organic layer was dried over anhydrous Na₂SO₄ and separated from the drying agent by atmospheric filtration. The filtrate was evaporated using a rotary evaporator under reduced pressure and subjected to column chromatography using hexane, ethyl acetate, and acetic acid (*v/v/v* = 50/50/1) as an eluent, followed by recrystallization from chloroform, generating the title molecule **1a** as a white solid in a 74% isolated yield (1.37 g, 4.2 mmol).

2.2.1. 2,3,5,6-Tetrafluoro-4-[2-(4-methoxyphenyl)ethyn-1-yl]benzoic acid (**1a**)

Yield: 74% (white solid); T_m : 223 °C (determined by POM); ¹H NMR (DMSO-*d*₆): δ 3.82 (s, 3H), 7.05 (d, $J = 8.8$ Hz, 2H), 7.59 (d, $J = 8.8$ Hz, 2H), 14.55 (brs, 1H); ¹³C NMR (DMSO-*d*₆): δ 55.4, 72.8 (t, $J = 4.4$ Hz), 103.5 (t, $J = 3.6$ Hz), 105.9 (t, $J = 17.6$ Hz), 111.9, 113.6 (t, $J = 17.6$ Hz), 114.7, 133.6, 143.7 (dm, $J = 253.1$ Hz), 146.0 (dm, $J = 250.8$ Hz), 160.0, 160.8; ¹⁹F NMR (DMSO-*d*₆, CFCl₃): δ -136.3 to -136.6 (m, 2F), -138.9 to -139.1 (m, 2F); IR (KBr): ν 3730, 2844, 2221, 1698, 1601, 1475, 1247, 1174, 990, 835 cm⁻¹; HRMS (FAB): [M⁺] calcd C₁₆H₈F₄O₃: 324.0410, found: 324.0413.

2.2.2. 2-[(4-Ethoxyphenyl)ethyn-1-yl]-2,3,5,6-tetrafluorobenzoic acid (**1b**)

Yield: 89% (white solid); T_m : 224 °C (determined by POM); ¹H NMR (acetone-*d*₆): δ 1.39 (t, $J = 7.2$ Hz, 3H), 4.12 (q, $J = 7.2$ Hz, 2H), 7.02 (d, $J = 8.8$ Hz, 2H), 7.58 (d, $J = 8.8$ Hz, 2H), 6.0–8.0 (brs, 1H); ¹³C NMR (acetone-*d*₆): δ 14.9, 64.5, 73.4 (t, $J = 3.6$ Hz), 105.0 (t, $J = 3.7$ Hz), 108.1 (t, $J = 17.6$ Hz), 113.5, 113.6 (t, $J = 17.6$ Hz), 115.9, 134.5, 145.5 (ddt, $J = 253.8$, 13.2, 5.9 Hz), 147.4 (ddt, $J = 250.9$, 14.7, 3.6 Hz), 160.2, 161.6; ¹⁹F NMR (acetone-*d*₆, C₆F₆): δ -136.92 (dd, $J = 20.7$, 10.9 Hz, 2F), -140.31 (dd, $J = 20.7$, 10.9 Hz, 2F); IR (KBr): ν 3750, 2984, 2212, 1706, 1601, 1479, 1178, 994, 844 cm⁻¹; HRMS (FAB): [M⁺] calcd C₁₇H₁₀F₄O₃: 338.0566, found: 338.0563.

2.2.3. 2,3,5,6-Tetrafluoro-4-[2-(4-propyloxy)ethyn-1-yl]benzoic acid (**1c**)

Yield: 83% (white solid); T_m : 220 °C (determined by POM); ^1H NMR (acetone- d_6): δ 1.03 (t, J = 7.2 Hz, 3H), 1.81 (sext., J = 7.2 Hz, 2H), 4.031 (t, J = 6.8 Hz, 2H), 7.04 (d, J = 8.8 Hz, 2H), 7.58 (d, J = 8.8 Hz, 2H), 5.0–10 (brs, 1H); ^{13}C NMR (acetone- d_6): δ 10.7, 23.1, 70.4, 73.4 (t, J = 4.4 Hz), 105.0 (t, J = 3.6 Hz), 108.1 (t, J = 17.6 Hz), 113.5, 113.8 (t, J = 16.9 Hz), 115.9, 134.5, 145.4 (ddt, J = 253.8, 13.9, 5.1 Hz), 147.4 (ddt, J = 250.9, 15.4, 3.6 Hz), 160.3, 161.8; ^{19}F NMR (acetone- d_6 , C_6F_6): δ -136.91 (dd, J = 20.7, 10.5 Hz, 2F), -140.3 (dd, J = 20.7, 10.5 Hz, 2F); IR (KBr): ν 3650, 2966, 2211, 1705, 1601, 1476, 1331, 1253, 993 cm^{-1} ; HRMS (FAB): $[\text{M}^+]$ calcd $\text{C}_{18}\text{H}_{12}\text{F}_4\text{O}_3$: 352.0723, found: 352.0733.

2.2.4. 2-[(4-Butoxyphenyl)ethyn-1-yl]-2,3,5,6-tetrafluorobenzoic acid (**1d**)

Yield: 78% (white solid); T_m : 178 °C (determined by POM); ^1H NMR (acetone- d_6): δ 0.97 (t, J = 7.2 Hz, 3H), 1.50 (sext., J = 7.2 Hz, 2H), 1.76 (quin, J = 7.2 Hz, 2H), 4.03 (t, J = 6.8 Hz, 2H), 6.98 (d, J = 8.8 Hz, 2H), 7.52 (d, J = 8.8 Hz, 2H), 10.0 (brs, 1H); ^{13}C NMR (CDCl_3): δ 14.1, 19.8, 31.9, 68.6, 73.4 (t, J = 5.1 Hz), 105.0 (t, J = 3.7 Hz), 108.1 (t, J = 16.1 Hz), 113.5, 113.5 (t, J = 16.2 Hz), 115.8, 134.4, 145.5 (ddt, J = 252.3, 13.2, 5.8 Hz), 147.3 (ddt, J = 253.0, 13.9, 3.6 Hz), 160.3, 161.7; ^{19}F NMR (acetone- d_6 , C_6F_6): δ -136.9 to -137.1 (m, 2F), -140.2 to -140.4 (m, 2F); IR (KBr): ν 3743, 2950, 2209, 1707, 1600, 1477, 1252, 1177, 993 cm^{-1} ; HRMS (FAB): $[\text{M}^+]$ calcd $\text{C}_{19}\text{H}_{14}\text{F}_4\text{O}_3$: 366.0879, found: 366.0893.

2.2.5. 2,3,5,6-Tetrafluoro-4-[2-(4-pentyloxy)ethyn-1-yl]benzoic acid (**1e**)

Yield: 44% (white solid); T_m : 175 °C (determined by POM); ^1H NMR (acetone- d_6): δ 0.94 (t, J = 7.2 Hz, 3H), 1.35–1.52 (m, 4H), 1.80 (quin, J = 6.8 Hz, 2H), 4.07 (t, J = 6.8 Hz, 2H), 7.01 (d, J = 8.8 Hz, 2H), 7.55 (d, J = 8.8 Hz, 2H), 9.07 (brs, 1H); ^{13}C NMR (acetone- d_6): δ 14.3, 23.1, 29.0, 29.7, 69.2, 73.5 (t, J = 4.4 Hz), 105.2 (t, J = 3.6 Hz), 108.4 (t, J = 18.3 Hz), 113.8, 113.9 (t, J = 17.6 Hz), 116.1, 134.6, 145.6 (ddt, J = 255.2, 15.3, 4.4 Hz), 147.6 (ddt, J = 250.9, 14.7, 3.6 Hz), 160.3, 162.0; ^{19}F NMR (acetone- d_6 , C_6F_6): δ -136.92 (dd, J = 20.7, 10.9 Hz, 2F), -140.28 (dd, J = 20.7, 10.9 Hz, 2F); IR (KBr): ν 3485, 2948, 2212, 1707, 1600, 1481, 1253, 1176, 996, 837 cm^{-1} ; HRMS (FAB): $[\text{M}^+]$ calcd $\text{C}_{20}\text{H}_{16}\text{F}_4\text{O}_3$: 380.1036, found: 380.1027.

2.2.6. 2,3,5,6-Tetrafluoro-4-[2-(4-hexyloxy)ethyn-1-yl]benzoic acid (**1f**)

Yield: 65% (white solid); T_m : 185 °C (determined by POM); ^1H NMR (acetone- d_6): δ 0.90 (t, J = 6.8 Hz, 3H), 1.30–1.38 (m, 4H), 1.48 (quin, J = 6.8 Hz, 2H), 1.79 (quin, J = 6.8 Hz, 2H), 4.06 (t, J = 6.8 Hz, 2H), 7.02 (d, J = 8.8 Hz, 2H), 7.57 (d, J = 8.8 Hz, 2H), 8.94 (brs, 1H); ^{13}C NMR (acetone- d_6): δ 14.3, 23.3, 26.4, 32.3, 68.9, 73.4 (t, J = 3.7 Hz), 105.0 (t, J = 3.6 Hz), 108.1 (t, J = 18.4 Hz), 113.5, 113.6 (t, J = 16.9 Hz), 115.9, 134.5, 145.5 (ddt, J = 252.3, 14.0, 5.1 Hz), 147.4 (ddt, J = 251.5, 14.7, 3.7 Hz), 160.2, 161.8; ^{19}F NMR (acetone- d_6 , C_6F_6): δ -136.97 (dd, J = 20.3, 12.4 Hz, 2F), -140.29 (dd, J = 20.3, 12.4 Hz, 2F); IR (KBr): ν 3450, 2946, 2211, 1705, 1602, 1476, 1329, 1172, 993, 834 cm^{-1} ; HRMS (FAB): $[\text{M}^+]$ calcd $\text{C}_{21}\text{H}_{18}\text{F}_4\text{O}_3$: 394.1192, found: 394.1202.

2.2.7. 2,3,5,6-Tetrafluoro-4-[2-(4-heptyloxy)ethyn-1-yl]benzoic acid (**1g**)

Yield: 75% (white solid); T_m : 172 °C (determined by POM); ^1H NMR (acetone- d_6): δ 0.89 (t, J = 6.8 Hz, 3H), 1.26–1.42 (m, 6H), 1.48 (quin, J = 6.8 Hz, 2H), 1.80 (quin, J = 6.8 Hz, 2H), 4.07 (t, J = 6.8 Hz, 2H), 7.03 (d, J = 8.8 Hz, 2H), 7.58 (d, J = 8.8 Hz, 2H), 6.0–10 (brs, 1H); ^{13}C NMR (acetone- d_6): δ 14.3, 23.3, 26.7, 29.8, 29.9, 32.6, 68.9, 73.4 (t, J = 4.4 Hz), 105.0 (t, J = 3.7 Hz), 108.1 (t, J = 17.6 Hz), 113.5, 113.7 (t, J = 16.9 Hz), 115.9, 134.5, 145.5 (ddt, J = 253.1, 13.9, 5.8 Hz), 147.4 (ddt, J = 250.8, 14.6, 3.7 Hz), 160.3, 161.8; ^{19}F NMR (acetone- d_6 , C_6F_6): δ -136.98 (dd, J = 20.4, 12.0 Hz, 2F), -140.31 (dd, J = 20.4, 12.0 Hz, 2F); IR (KBr): ν 3680, 2948, 2211, 1704, 1601, 1479, 1330, 1254, 1171, 995, 836 cm^{-1} ; HRMS (FAB): $[\text{M}^+]$ calcd $\text{C}_{22}\text{H}_{20}\text{F}_4\text{O}_3$: 408.1349, found: 408.1343.

2.2.8. 2,3,5,6-Tetrafluoro-4-[2-(4-octyloxy)ethyn-1-yl]benzoic acid (**1h**)

Yield: 41% (white solid); T_m : 167 °C (determined by POM); ^1H NMR (DMSO- d_6): δ 0.86 (t, J = 6.8 Hz, 3H), 1.23–1.34 (m, 8H), 1.40 (quin, J = 6.8 Hz, 2H), 1.72 (quin, J = 6.8 Hz, 2H), 4.02 (t, J = 6.8 Hz, 2H), 7.02 (d, J = 8.8 Hz, 2H), 7.56 (d, J = 8.8 Hz, 2H), 14.6 (brs, 1H); ^{13}C NMR (DMSO- d_6): δ 13.9, 22.0, 25.4, 24.5, 28.6, 28.7, 31.2, 67.8, 72.8 (t, J = 4.4 Hz), 103.6 (t, J = 3.6 Hz), 106.0 (t, J = 16.9 Hz), 111.8, 113.6 (t, J = 17.6 Hz), 115.2, 133.6, 142.3–145.2 (m, 1C), 144.5–147.4 (m, 1C), 160.0, 160.3; ^{19}F NMR (DMSO- d_6 , CFCl_3): δ -136.49 (dd, J = 23.3, 10.9 Hz, 2F), -140.50 (dd, J = 23.3, 10.9 Hz, 2F); IR (KBr): ν 3673, 2946, 2210, 1704, 1600, 1477, 1329, 1253, 1170, 995, 836 cm^{-1} ; HRMS (FAB): $[\text{M}^+]$ calcd $\text{C}_{23}\text{H}_{22}\text{F}_4\text{O}_3$: 422.1505, found: 422.1510.

2.3. Single-Crystal X-ray Diffraction

Single-crystal X-ray diffraction (XRD) spectra were recorded using an XtaLAB AFC11 diffractometer (Rigaku, Tokyo, Japan). The reflection data were integrated, scaled, and averaged using the CrysAlisPro program (ver. 1.171.39.43a; Rigaku Corporation, Akishima, Japan), while empirical absorption corrections were applied using the SCALE 3 AB-SPACK scaling algorithm (CrysAlisPro). The structures were identified by a direct method (SHELXT-2018/2 [19]) and refined using the full matrix least-squares method (SHELXL-2018/3 [20]) visualized by Olex2 [21]. Crystallographic data were deposited in the Cambridge Crystallographic Data Centre (CCDC) database (CCDC 2193549 for **1a** and 2193550 for **1e**), which were obtained free of charge from the CCDC at www.ccdc.cam.ac.uk/data_request/cif (accessed on 23 November 2022).

2.4. Phase Transition Behavior

The phase transition behaviors were observed by POM using an Olympus BX53 microscope (Tokyo, Japan) equipped with a cooling and heating stage (10002L, Linkam Scientific Instruments, Surrey, UK). Thermodynamic characterization was performed by differential scanning calorimetry (DSC; DSC-60 Plus, Shimadzu, Kyoto, Japan) at heating and cooling rates of 5.0 °C min^{-1} under N_2 .

2.5. Photophysical Properties

Ultraviolet–visible (UV–vis) absorption spectra were recorded using a JASCO V-750 absorption spectrometer (JASCO, Tokyo, Japan). The PL spectra of the solutions were measured using an FP-6600 fluorescence spectrometer (JASCO, Tokyo, Japan). The PL quantum yields were measured using a Quantaurus-QY C11347-01 instrument (Hamamatsu Photonics, Hamamatsu, Japan).

2.6. Theoretical Calculations

All computations were performed using Gaussian 16 program set [22] with the density functional theory (DFT) at the M06-2X hybrid functional [23] and 6-31+G(d,p) (for all atoms) basis set with a conductor-like polarizable continuum model (CPCM) [24] for CH_2Cl_2 . Theoretical vertical transitions were also calculated using the time-dependent DFT (TD-DFT) method at the same theory level using the same solvation model.

3. Results and Discussion

3.1. Synthesis and Crystal Structure

We first synthesized the fluorinated tolanecarboxylic acid **1** from the corresponding ester **2** via hydrolysis under basic conditions; synthesis of **2** was previously accomplished (Figure 3) [12].

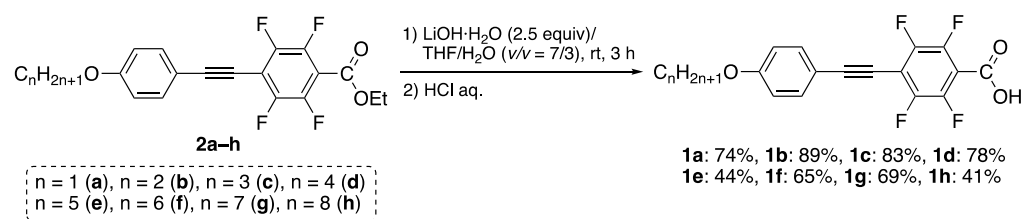


Figure 3. Synthetic procedure of **1a–h** from the corresponding ester **2**.

Treatment of ester **2a** with 2.5 equivalent of LiOH·H₂O in a mixed solvent of THF and H₂O (*v/v* = 7/3) at room temperature for 3 h underwent a hydrolysis reaction, which proceeded smoothly. Subsequently, treatment with an aqueous solution of concentrated HCl produced corresponding fluorinated tolanecarboxylic acid **1a**. The product was purified by column chromatography and recrystallization, and the resulting **1a** was generated as a white solid in a 74% isolated yield. Using a similar synthetic procedure, other analogs **1b–h** bearing various alkoxy chains were also produced in 41–89% isolated yields. The molecular structures of **1a–h** were assessed by ¹H, ¹³C, and ¹⁹F-NMR, along with IR and HRMS. All structures were completely identified and sufficiently pure to evaluate their phase transition and photophysical behaviors.

Among the fluorinated carboxylic acids **1a–h**, methoxy-substituted **1a** and pentyloxy-substituted **1e** afforded single crystals that were appropriate for X-ray crystallographic analysis. Figure 4 shows the crystal structures of **1a** and **1e** and their packing structures.

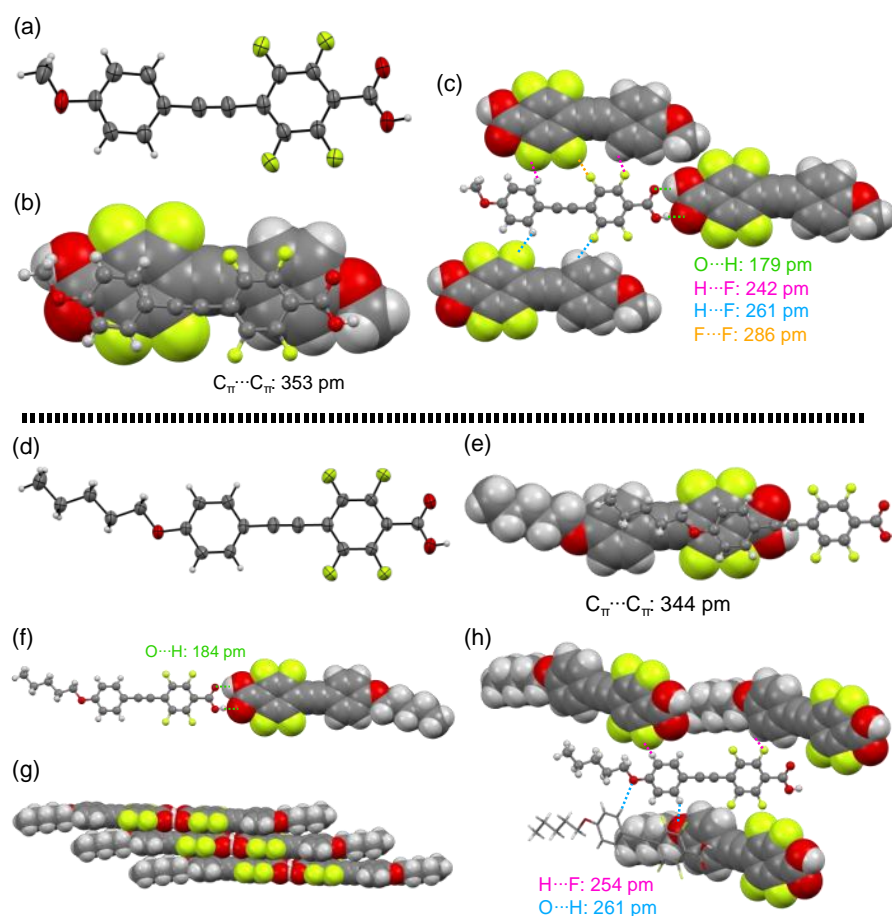


Figure 4. (a) Crystal structure of **1a** with an ORTEP drawing and (b,c) packing structures. (d) Crystal structure of **1e** with an ORTEP drawing and (e–h) packing structures.

Methoxy-substituted **1a** crystallized with a triclinic system in the $P\bar{1}$ space group and two molecular units were contained in the Cry lattice. The dihedral angle between two aromatic rings in the tolane scaffold was only 4.7° , almost coplanar to each other (Figure 4a). The dihedral angle between the fluorinated aromatic ring and the carbonyl plane was reported 34° for the ester precursor **2a** [12]. However, the dihedral angle of the carboxylic acid **1a** was only 3.7° , resulting in an almost coplanar structure. With respect to the packing structures, the two planar tolane scaffolds were arranged in a layer structure with an antiparallel direction. This phenomenon is caused by the electrostatic weak π - π interaction (short contact of $C\pi \cdots C\pi$: 353 pm) between the electron-rich methoxy-substituted aromatic ring and the electron-deficient fluorinated aromatic ring (Figure 4b). Additionally, the fluorinated tolanecarboxylic acid **1a** formed plural intermolecular interactions (Figure 4c), such as $O \cdots H$ hydrogen bond (short contact of $O \cdots H$: 179 pm), $H \cdots F$ hydrogen bond (short contact of $H \cdots F$: 242 and 261 pm), and $F \cdots F$ interaction (short contact of $F \cdots F$: 286 pm), wherein the short contacts mentioned above were almost identical or below the sum of van der Waals radii [25].

In contrast, pentyloxy-substituted **1e** furnished single crystals with a monoclinic system in the $C2/c$ space group, and eight molecular units were contained in the Cry lattice. The electron-rich aromatic ring and the electron-deficient fluorinated aromatic ring were nearly coplanar, with a deviation of 3.0° . The dihedral angle between the fluorinated aromatic ring and the carbonyl plane was 11° , being almost coplanar (Figure 4d). However, unlike the π - π stacking of the antiparallel orientation in **1a**, **1e** formed a slipped π - π stacking (short contact of $C\pi \cdots C\pi$: 344 pm) with a synparallel orientation induced by the electrostatic interaction between the electron-rich pentyloxy aromatic ring and the electron-deficient fluorinated aromatic ring (Figure 4e). As shown in Figure 4f,g, the carboxyl units in **1e** also formed an intermolecular $O \cdots H$ hydrogen bond with a short contact of 184 pm, leading to formation of layer structures. For construction of the crystal structure of **1e**, more intermolecular interactions, such as additional $O \cdots H$ and $H \cdots F$ hydrogen bonds (Figure 4h), were also observed. The interatomic distance was 254 and 261 pm for $O \cdots H$ and $H \cdots F$, respectively, which was also almost identical or below the sum of van der Waals radii [25].

3.2. Phase Transition Behavior

With the fluorinated tolanecarboxylic acids, **1a–h**, in hand, we evaluated their phase transition behavior using DSC and POM. Table 1 summarizes the phase sequence and phase transition temperature for **1a–h** during the first heating and cooling process determined by POM. Subsequent phase transition behavior is listed in Table S2 (ESI). Figure 5 shows the POM texture images of **1d–h** observed in the mesophase.

Table 1. The phase transition behavior of the fluorinated tolanecarboxylic acids, **1a–h**, during the first heating and cooling process observed by POM.

Molecule	Phase Sequence and Phase Transition Temperature [$^\circ\text{C}$] ¹	
	Heating Process	Cooling Process
1a	Cry 224 Iso	Iso 165 G
1b	Cry 207 Iso	Iso 140 G
1c	Cry 211 Iso	Iso 158 G
1d	Cry 176 N 198 Iso	Iso 124 G
1e	Cry ¹ 160 Cry ² 170 N 191 Iso	Iso 132 G
1f	Cry 181 N 190 Iso	Iso 141 G
1g	Cry 169 N 184 Iso	Iso 150 G
1h	Cry 161 N 186 Iso	Iso 146 N 118 G

¹ Determined by POM. Abbreviations: Cry: crystalline; G: Glassy; N: nematic; and Iso: isotropic phases.

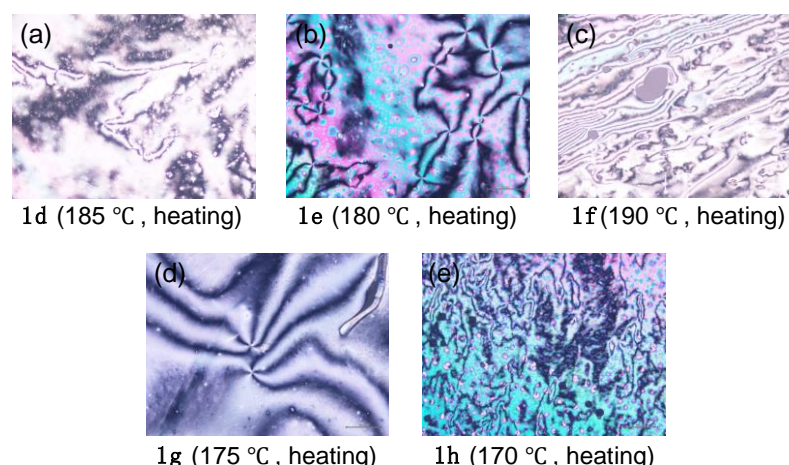


Figure 5. Optical microphotographs of (a) **1d**, (b) **1e**, (c) **1f**, (d) **1g**, and (e) **1h** in the mesophase phase.

The DSC measurement of methoxy-substituted **1a** showed a large endothermic peak with an onset temperature of 223 °C during the first heating process. No sharp exothermic peak due to the Iso → Cry phase transition was observed during the subsequent cooling process. As a result of POM observation, however, a phase transition from the Iso phase to a glassy amorphous solid (G) phase was observed; **1a** did not show any mesophase (Figure S25). The POM observation also proved that **1a** showed no mesophase between the Cry and isotropic (Iso) phases. Additionally, no mesophase was observed for ethoxy-substituted **1b** and propoxy-substituted **1c** by POM and DSC measurements. In contrast, butoxy-substituted **1d** showed an endothermic phase transition between the Cry and Iso phases in the first heating process of the DSC measurement and a bright-viewing field with fluidity during the heating and cooling processes of the POM observation. Thus, the phase transition behavior of butoxy-substituted **1d** possessed the LC characteristic. A four-brush Schlieren texture was observed as the optical image (Figure 5a), which is a typical texture for the N LC phase. During the subsequent cooling process, however, only the Iso → G phase transition was observed. The phase transition behavior was also supported by temperature-varying powder X-ray diffraction (VT-PXRD) measurements (Figure S26). Further POM observation was found to show similar phase transition between G and Iso phases during the second cycles. Similar to **1d**, molecules **1e** and **1f** also exhibited an N-phase during the first heating process (Figure 5b,c), while, after the first cooling process, the LC phase disappeared, showing only a phase transition between the G and Iso phases. The other analogs, viz., **1g** and **1h**, with a relatively long alkoxy chain, were found to show a mesophase during both heating and cooling processes due to increasing stabilization of the mesophase. Thus, both **1g** with a C₇H₁₅ chain and **1h** with a C₈H₁₅ chain exhibited an N-phase with a four-brush Schlieren texture through POM measurements during both heating and cooling cycles (Figure 5d,e), in which the observed mesophase can be assigned as an N-phase by the VT-PXRD measurements (Figure S26). Focusing on the melting temperature (T_m), which is defined as the phase transition temperature from Cry to Iso or LC phases, the T_m of **1a–h** was in the range of 167–224 °C for the heating process, which was much higher than that of the corresponding ester derivatives **2a–h** (34–109 °C) [12]. Unlike the ester derivatives, the carboxylic acids exhibited LC phases even with relatively short alkoxy chains, particularly C₄H₉O, due to the increased aspect ratio of the mesogenic core induced by formation of a dimeric structure through hydrogen bonds.

3.3. Photophysical Behavior in Solution Phase

A solution sample was prepared to investigate the photophysical behavior of the fluorinated carboxylic acids, **1a–h**, in the solution phase by individually dissolving **1a–h** in CH₂Cl₂; the concentration was adjusted to 1.0 × 10^{−5} mol L^{−1}. Figure 6 illustrates the

photophysical behavior in the solution, and the photophysical data are summarized in Table 2.

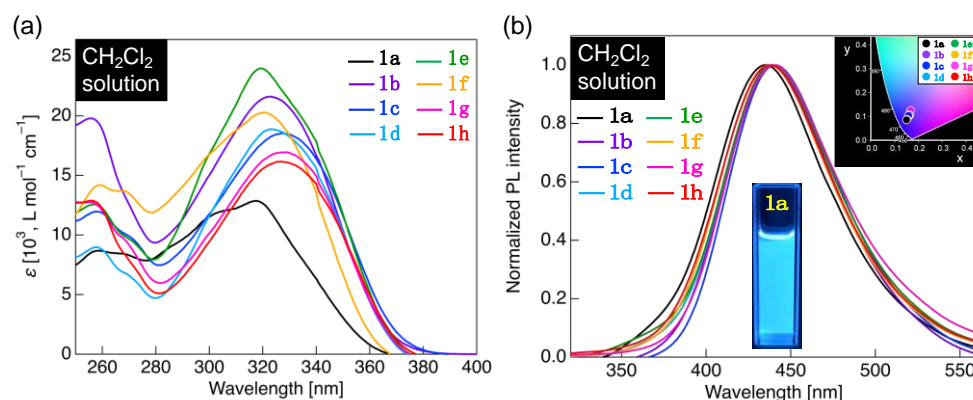


Figure 6. (a) Ultraviolet (UV)–visible absorption spectrum of **1a–h** in the CH_2Cl_2 solution (concentration: $1.0 \times 10^{-5} \text{ mol L}^{-1}$). (b) PL spectrum of **1a–h** in the CH_2Cl_2 solution (concentration: $1.0 \times 10^{-5} \text{ mol L}^{-1}$) and a photograph of the PL behavior of **1a** solution under UV light ($\lambda_{\text{ex}} = 365 \text{ nm}$). Inset: Commission Internationale de l’Eclairage (CIE) diagram for PL color of **1a–h** solutions.

Table 2. Photophysical data of **1a–h** in solution state.

Molecule	Solvent (E_{T30})	λ_{abs} [nm] ¹ (ϵ , 10^3 [L mol ⁻¹ cm ⁻¹])	λ_{PL} [nm] ¹ (Φ_{PL}) ²	CIE Coordinate (x, y)
1a	CH_2Cl_2 (40.7)	259 (8.69), 317 (12.9)	435 (0.33)	(0.150, 0.085)
	Toluene (33.9)	324 (27.3)	403 (0.35)	(0.160, 0.029)
	CHCl_3 (39.1)	274 (36.0), 284 (36.2) 317 (27.7)	420 (0.33)	(0.155, 0.051)
	MeCN (45.6)	256 (14.2), 299sh (26.3), 314 (30.2)	463 (0.10)	(0.194, 0.238)
1b	CH_2Cl_2 (40.7)	256 (19.8), 323 (21.6)	439 (0.33)	(0.152, 0.088)
1c	CH_2Cl_2 (40.7)	258 (12.0), 327 (18.5)	441 (0.35)	(0.158, 0.103)
1d	CH_2Cl_2 (40.7)	258 (8.98), 323 (18.9)	439 (0.37)	(0.161, 0.108)
1e	CH_2Cl_2 (40.7)	257 (12.6), 319 (24.0)	440 (0.27)	(0.160, 0.107)
1f	CH_2Cl_2 (40.7)	259 (14.2), 320 (20.3)	437 (0.33)	(0.160, 0.101)
1g	CH_2Cl_2 (40.7)	255 (12.8), 329 (16.9)	440 (0.38)	(0.167, 0.125)
1h	CH_2Cl_2 (40.7)	256 (12.9), 327 (16.2)	438 (0.37)	(0.163, 0.105)

¹ Concentration: $1.0 \times 10^{-5} \text{ mol L}^{-1}$. ² Measured using an integrating sphere.

Methoxy-substituted **1a** in CH_2Cl_2 absorbed UV light with a maximum absorption wavelength (λ_{abs}) near 259 nm and 317 nm (Figure 6a). Other analogs, particularly **1b–h**, also showed two absorption bands: a high-energy absorption band near 255–259 nm of λ_{abs} and a low-energy absorption band near 319–329 nm of λ_{abs} (Figure 6a). Quantum chemical calculations were performed by the TD-DFT method using **1a** as a representative, and two allowed transitions with theoretical absorption wavelengths of 319 and 262 nm were calculated as theoretical vertical transitions (Figure S31). The calculated absorption wavelengths were close to the experimentally obtained λ_{abs} . Thus, the result confirms that the long-wavelength absorption band of **1a** in CH_2Cl_2 is the $\pi\pi^*$ transition with an intramolecular charge transfer (ICT) character involving the highest occupied molecular orbital to the lowest unoccupied molecular orbital (HOMO \rightarrow LUMO) transition, while the short-wavelength band is the $\pi\pi^*$ transition with a local excitation character involving a HOMO–1 \rightarrow LUMO transition.

With the λ_{abs} as the excitation wavelength, the methoxy-substituted **1a** in the solution state was observed to emit blue PL, with a maximum PL wavelength (λ_{PL}) of approximately 435 nm (Figure 6b). In addition, **1b–h** with varying lengths of alkoxy group were found to have a PL band with λ_{PL} in the range of 437–441 nm, leading to the blue PL. Considering the observed PL colors using the Commission Internationale de l’Eclairage (CIE) diagrams

(Figure 6b, inset), the CIE coordinates for the PL colors of **1a–h** were similar to each other. The PL color of the fluorinated tolanecarboxylic acids in CH_2Cl_2 showed a uniform blue PL in the solution state without affecting the alkoxy-chain length. PL quantum yields (Φ_{PL}) of **1a–h** in CH_2Cl_2 solutions were in the range of 0.27–0.38, which is higher than that of the unsubstituted tolane [26,27]. This phenomenon is observed because the donor– π –acceptor structure of the fluorinated tolanecarboxylic acid suppresses the internal conversion from the $\pi\pi^*$ excited state to the dark $\pi\sigma^*$ excited state. In addition, we investigated the effect of solvent polarity on photophysical properties using **1a** as a representative [28]. We found that, although the solvent polarity did not affect the absorption properties significantly, the PL properties shifted to longer wavelengths as the polarity increased, which is attributed to stabilization of solute–solvent interactions (Figure S28d). Considering the Lippert–Mataga plot [29,30], which is created from the orientational polarizability (Δf) and Stokes shift ($\Delta\nu$) on the horizontal and vertical axes, respectively, a linear relationship was obtained (Figure S28e). The dipole moment difference ($\mu_e - \mu_g$) between the excited and ground states was 14.1 D, which was calculated from the slope of the straight line. The large difference in the dipole moment proves that the radiative deactivation from the ICT excited state resulted in the PL of **1a–h**.

3.4. Photophysical Behavior in Aggregated Phases

We next examined the PL behavior of fluorinated tolanecarboxylic acids, **1a–h**, in the aggregated phases. Figure 7 shows the PL spectrum, photographs of the PL behavior under UV irradiation, and a CIE diagram for the PL colors. The photophysical data of **1a–h** in the aggregated phases are summarized in Table 3.

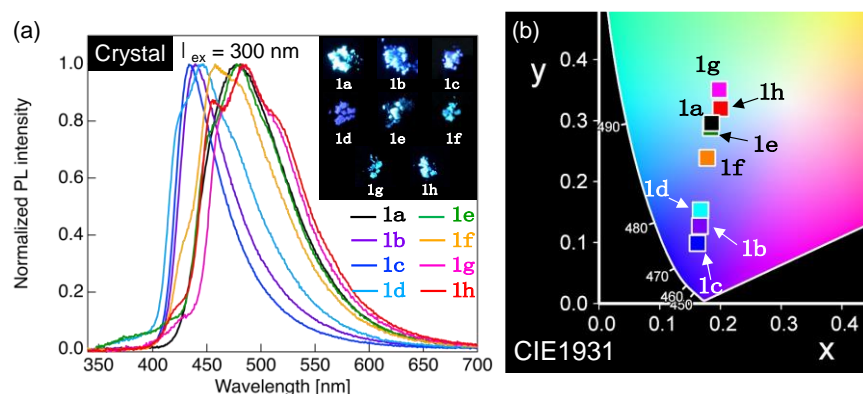


Figure 7. (a) PL spectra of **1a–h** in crystalline state. Excitation wavelength (λ_{ex}): 300 nm. Inset: Photographs of the PL behavior of the **1a–h** crystals under UV light ($\lambda_{\text{ex}} = 365$ nm). (b) CIE color diagram of PL colors for **1a–h** crystals.

Table 3. Photophysical data of **1a–h** in aggregated phases.

Molecule	Phase ¹	λ_{PL} [nm] (Φ_{PL}) ²	CIE Coordinate (x, y)
1a	Crystalline (Cry)	481 (0.99)	(0.185, 0.296)
1b	Cry	440 (0.69)	(0.166, 0.127)
1c	Cry	434 (0.71)	(0.162, 0.099)
1d	Cry	428sh, 446(0.63)	(0.167, 0.153)
1e	Cry	454sh, 478 (0.57)	(0.184, 0.288)
1f	Cry	430sh, 458, 480sh (0.60)	(0.178, 0.239)
1g	Cry	465sh, 482, 511sh (0.49)	(0.198, 0.351)
1h	Cry	455, 483, 511sh (0.70)	(0.200, 0.320)
1h	– ³	428sh, 454, 479 (0.12)	(0.189, 0.240)

¹ Unless mentioned otherwise, the crystalline sample prepared by column chromatography and recrystallization was used. Measured at 25 °C. ² Measured using an integrating sphere. ³ Samples with mesophase aggregate structures were prepared by quenching and immersing mesophase (170 °C) during the 1st heating process in liquid nitrogen to maintain the mesophase molecular aggregates at room temperature.

When methoxy-substituted **1a** in the Cry phase was excited by irradiation with incident light of 300 nm, which is the maximum excitation wavelength (λ_{ex}), a single PL band was observed with a λ_{PL} of approximately 481 nm (Figure 7a). As shown in Figure 8b,c, the CIE coordinate (x, y) of the PL color was (0.185, 0.296), indicating that the PL color was light blue. Notably, a CH_2Cl_2 solution of **1a** had a Φ_{PL} of 0.33, whereas the **1a** in the Cry phase dramatically increased the Φ_{PL} to up to 0.99. Although **1b–h** with varying lengths of the alkoxy chain had almost identical λ_{PL} in dilute solutions, they exhibited various λ_{PL} in the Cry phase, ranging from 428 to 511 nm (Figure 7a). The alteration in λ_{PL} indicated a change in the PL color. Thus, various PL colors ranging from blue to light green were obtained by changing the length of the alkoxy chain, which is evident from the photographs and the CIE diagram demonstrating the PL colors (Figure 7b). The Φ_{PL} values of **1b–h** in the Cry phase were in the range of 0.49–0.71, which were higher than those in dilute solutions (up to 0.38). Considering the crystal packing structures of **1a** and **1e** shown in Figure 4, the change in the length of the alkoxy chain considerably altered the molecular arrangements in molecular aggregated phases; **1a–h** exhibited various PL behaviors in the Cry phase. Furthermore, $\text{O} \cdots \text{H}$ and $\text{H} \cdots \text{F}$ hydrogen bonds and intermolecular interactions, such as $\text{F} \cdots \text{F}$ interactions and weak $\pi \cdots \pi$ interactions, function in the Cry phase, which possibly restricts the molecular motion to suppress non-radiative deactivation, resulting in a significant increase in the Φ_{PL} in the Cry state.

The PL behavior in the aggregated structures of the N-phase was evaluated using octyloxy-substituted **1h** with an N LC phase. The measurement sample was prepared by quenching the sample with the N LC phase at 170 °C, which was developed during the 1st heating process, with liquid nitrogen. Figure 8 shows the PL spectra and CIE diagrams for **1h** with the Cry- and N-phase molecular aggregated structures.

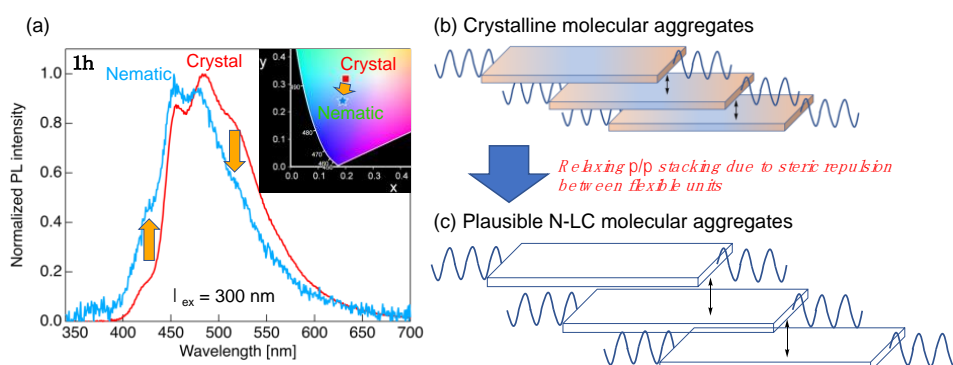


Figure 8. (a) PL spectra of **1h** with the Cry- and N-phase molecular aggregated structures. Inset: CIE diagram of the PL colors for **1h** with the Cry- and N-phase aggregated structures. (b,c) Schematic illustration of plausible structural alteration from the Cry- to N-phase molecular aggregated structures.

The PL spectrum of **1h** with N-phase aggregated structures was also obtained by irradiation with incident light of 300 nm, in which the λ_{PL} was approximately 454 and 479 nm, along with a shoulder peak of approximately 428 nm. Compared to the Cry phase, the PL spectra of the N-phase aggregated structure yielded a slight short-wavelength shift with weakened long-wavelength shoulder peaks and increased short-wavelength peaks. In the Cry phase, the dimer mesogens formed a dense packing structure due to the weak $\pi \cdots \pi$ interactions (Figure 8b), as shown in Figure 4g. Conversely, the phase transition to the N-phase increased the molecular fluidity, allowing the increase in the two molecular distances (Figure 8c). The increased spacing between the dimer mesogens in the N-phase aggregated structure and the promotion of the molecular motion drastically reduced the Φ_{PL} compared to that in the Cry phase.

4. Conclusions

In conclusion, we designed and synthesized a series of fluorinated tolanecarboxylic acids bearing various lengths of alkoxy chains and investigated their phase transition and photophysical behaviors. The fluorinated tolanecarboxylic acids exhibited the N LC phase due to formation of the dimer-type mesogen of the carboxylic acid moiety via O···H hydrogen bonds. Furthermore, regarding photophysical measurements, the fluorinated tolanecarboxylic acids emitted blue PL in the solution phase. The PL quantum yield (Φ_{PL}) was approximately 0.33, which was higher than that of the unsubstituted tolane. The fluorinated tolanecarboxylic acid exhibited remarkably strong PL even in the Cry phase, and its Φ_{PL} was much higher than that in the dilute-solution state, which could be attributed to the O···H and H···F hydrogen bonds and the weak π ··· π and F···F intermolecular interactions. Investigation of the PL behavior in the N-phase molecular aggregated structure revealed a slight short-wavelength shift and a significant decrease in Φ_{PL} , which is attributable to the wider spacing between the dimer-type mesogens caused by increasing the molecular fluidity in the N-phase. These findings will offer a new molecular design for PLLC molecules effectively using intermolecular interactions and pave the way for developing new thermo-responsive luminescent materials in the future.

Supplementary Materials: The following supporting information can be downloaded at: <https://www.mdpi.com/article/10.3390/cryst13010025/s1>, Figures S1–S24: NMR spectra of **1a–h**; Figure S25: DSC thermograms of **1a–h**; Figure S26: TG thermograms of **1a–h**; Figure S27: PXRD patterns of **1d–h** on the mesophase; Figure S28: UV–vis absorption and PL spectra of **1a–h** in CH₂Cl₂ solution; Figure S29: UV–vis absorption and PL spectra of **1a** in different solvents; Figure S30: Excitation and PL spectra of **1a–h** in the Cry phase; Figure S31: Excitation and PL spectra of **1h** in the aggregated structure of the nematic phase; Figures S32 and S33: Optimized structure of **1a** and **1e** and their orbital distributions; Table S1: Crystallographic data of **1a** and **1e**; Table S2: Phase transition behaviors of **1a–h** observed by DSC measurements; Table S3: Solvent effect on the photophysical behavior; Tables S4 and S5: Cartesian coordinate for **1a** and **1e**.

Author Contributions: Conceptualization, S.Y.; methodology, S.Y.; validation, S.Y., M.K., K.Y. and T.K.; investigation, S.Y., M.K. and K.Y.; resources, S.Y. and T.K.; data curation, S.Y.; writing—original draft preparation, S.Y. and M.K.; writing—review and editing, S.Y., M.K., K.Y., M.N., T.A., H.F. and T.K.; visualization, S.Y.; supervision, S.Y.; project administration, S.Y.; funding acquisition, S.Y. All authors have read and agreed to the published version of the manuscript.

Funding: This research was partially funded by the Murata Science Foundation and Shorai Foundation for Science and Technology.

Data Availability Statement: Not applicable.

Acknowledgments: We are deeply grateful to Sakurai and Shimizu (Kyoto Inst. Tech.) for their valuable cooperation in the PXRD measurements.

Conflicts of Interest: The authors declare no conflict of interest.

References

1. Irfan, M.; Sumra, I.; Zhang, M.; Song, Z.; Liu, T.; Zeng, Z. Thermochromic and highly tunable color emitting bis-tolane based liquid crystal materials for temperature sensing devices. *Dye. Pigment.* **2021**, *190*, 109272. [[CrossRef](#)]
2. Kato, T.; Uchida, J.; Ichikawa, T.; Sakamoto, T. Functional liquid crystals towards the next generation of materials. *Angew. Chem. Int. Ed.* **2018**, *57*, 4355–4371. [[CrossRef](#)] [[PubMed](#)]
3. Wang, Y.; Shi, J.; Chen, J.; Zhu, W.; Baranoff, E. Recent progress in luminescent liquid crystal materials: Design, properties and application for linearly polarized emission. *J. Mater. Chem. C* **2015**, *3*, 7993–8005. [[CrossRef](#)]
4. Sagara, Y.; Kato, T. Stimuli-responsive luminescent liquid crystals: Change of photoluminescent colors triggered by a shear-induced phase transition. *Angew. Chem. Int. Ed.* **2008**, *120*, 5253–5256. [[CrossRef](#)]
5. Zhao, D.; Fan, F.; Cheng, J.; Zhang, Y.; Wong, K.S.; Chigrinov, V.G.; Kwok, H.S.; Guo, L.; Tang, B.Z. Light-emitting liquid crystal displays based on an aggregation-induced emission luminogen. *Adv. Opt. Mater.* **2015**, *3*, 199–202. [[CrossRef](#)]
6. Yamada, S.; Miyano, K.; Konno, T.; Agou, T.; Kubota, T.; Hosokai, T. Fluorine-containing bistolanes as light-emitting liquid crystalline molecules. *Org. Biomol. Chem.* **2017**, *15*, 5949–5958. [[CrossRef](#)]

7. Morita, M.; Yamada, S.; Agou, T.; Kubota, T.; Konno, T. Luminescence tuning of fluorinated bistolanes via electronic or aggregated-structure control. *Appl. Sci.* **2019**, *9*, 1905. [[CrossRef](#)]
8. Morita, M.; Yamada, S.; Konno, T. Fluorine-induced emission enhancement of tolans via formation of tight molecular aggregates. *New J. Chem.* **2020**, *44*, 6704–6708. [[CrossRef](#)]
9. Morita, M.; Yamada, S.; Konno, T. Systematic studies on the effect of fluorine atoms in fluorinated tolans on their photophysical properties. *Molecules* **2021**, *26*, 2274. [[CrossRef](#)]
10. Yamada, S.; Kobayashi, K.; Morita, M.; Konno, T. D- π -A-type fluorinated tolans with a diphenylamio group: Crystal polymorphism formation and photophysical behavior. *CrystEngComm* **2022**, *24*, 936–941. [[CrossRef](#)]
11. Morita, M.; Yamada, S.; Konno, T. Halogen atom effect of fluorinated tolans on their luminescence characteristics. *New J. Chem.* **2022**, *46*, 4562–4569. [[CrossRef](#)]
12. Yamada, S.; Kataoka, M.; Yoshida, K.; Nagata, M.; Agou, T.; Fukumoto, H.; Konno, T. Photophysical and thermophysical behavior of D-p-A-type fluorinated diphenylacetylenes bearing an alkoxy and an ethoxycarbonyl group at both longitudinal molecular terminals. *J. Fluor. Chem.* **2022**, *261–262*, 110032. [[CrossRef](#)]
13. Yamada, S.; Uto, E.; Sakurai, T.; Konno, T. Development of thermoresponsive near-ultraviolet photoluminescent liquid crystals using hexyloxy-terminated fluorinated tolane dimers connected with an alkylene spacer. *J. Mol. Liq.* **2022**, *362*, 119755. [[CrossRef](#)]
14. Yamada, S.; Uto, E.; Yoshida, K.; Sakurai, T.; Konno, T. Development of photoluminescent liquid-crystalline dimers bearing two fluorinated tolane-based luminous mesogens. *J. Mol. Liq.* **2022**, *363*, 119884. [[CrossRef](#)]
15. Arakawa, Y.; Sasaki, Y.; Igawa, K.; Tsuji, H. Hydrogen bonding liquid crystalline benzoic acids with alkylthio groups: Phase transition behavior and insights into the cybotactic nematic phase. *New J. Chem.* **2017**, *41*, 6514–6522. [[CrossRef](#)]
16. Arakawa, Y.; Kang, S.; Watanabe, J.; Konishi, G. Assembly of thioether-containing rod-like liquid crystalline materials assisted by hydrogen-bonding terminal carboxyl groups. *RSC Adv.* **2015**, *5*, 8056–8062. [[CrossRef](#)]
17. Wen, J.; Tian, M.; Yu, H.; Guo, Z.; Chen, Q. Novel fluorinated liquid crystals. Part 9.—Synthesis and mesomorphic properties of 4-(*n*-alkoxycarbonyl)phenyl 4-[(4-*n*-alkoxy-2,3,5,6-tetrafluorophenyl)ethynyl]benzoates. *J. Mater. Chem.* **1994**, *4*, 327–330. [[CrossRef](#)]
18. Wen, J.X.; Tian, M.Q.; Chen, Q. Synthesis and mesomorphic properties of 4'-*n*-alkoxy-2,3,5,6-tetrafluorobiphenyl-4-carboxylic acids. *J. Fluor. Chem.* **1994**, *67*, 207–210. [[CrossRef](#)]
19. Sheldrick, G.M. SHELXT-Integrated space-group and crystal-structure determination. *Acta Crystallogr. Sect. A Found. Adv.* **2015**, *71*, 3–8. [[CrossRef](#)]
20. Sheldrick, G.M. Crystal structure refinement with SHELXL. *Acta Crystallogr. Sect. C Struct. Chem.* **2015**, *71*, 3–8. [[CrossRef](#)]
21. Dolomanov, O.V.; Bourhis, L.J.; Gildea, R.J.; Howard, J.A.K.; Puschmann, H. OLEX2: A complete structure solution, refinement, and analysis program. *J. Appl. Crystallogr.* **2009**, *42*, 339–341. [[CrossRef](#)]
22. Frisch, M.J.; Trucks, G.W.; Schlegel, H.B.; Scuseria, G.E.; Robb, M.A.; Cheeseman, J.R.; Scalmani, G.; Barone, V.; Petersson, G.A.; Nakatsuji, H.; et al. *Gaussian 16, Revision B.01*; Gaussian, Inc.: Wallingford, CT, USA, 2016.
23. Hohenstein, E.G.; Chill, S.T.; Sherrill, C.D. Assessment of the performance of the M05-2X and M06-2X exchange-correlation functionals for noncovalent interactions in biomolecules. *J. Chem. Theory Comput.* **2008**, *4*, 1996–2000. [[CrossRef](#)] [[PubMed](#)]
24. Li, H.; Jensen, J.H. Improving the efficiency and convergence of geometry optimization with the polarizable continuum model: New energy gradients and molecular surface tessellation. *J. Comput. Chem.* **2004**, *25*, 1449–1462. [[CrossRef](#)] [[PubMed](#)]
25. Bondi, A. van der Waals volumes and radii. *J. Phys. Chem.* **1964**, *68*, 441–451. [[CrossRef](#)]
26. Zgierski, M.Z.; Lim, E.C. Nature of the 'dark' state in diphenylacetylene and related molecules: State switch from the linear $\pi\pi^*$ state to the bent $\pi\sigma^*$ state. *Chem. Phys. Lett.* **2004**, *387*, 352–355. [[CrossRef](#)]
27. Saltiel, J.; Kumar, V.K.R. Photophysics of diphenylacetylene: Light from the "dark state". *J. Phys. Chem. A* **2012**, *116*, 10548–10558. [[CrossRef](#)]
28. Reichardt, C. Solvatochromic dyes as solvent polarity indicators. *Chem. Rev.* **1994**, *94*, 2319–2358. [[CrossRef](#)]
29. Mataga, N.; Kaifu, Y.; Koizumi, M. The solvent effect on fluorescence spectrum, change of solute-solvent interaction during the lifetime of excited solute molecule. *Bull. Chem. Soc. Jpn.* **1955**, *28*, 690–691. [[CrossRef](#)]
30. Mataga, N.; Kaifu, Y.; Koizumi, M. Solvent effects upon fluorescence spectra and dipole moments of excited molecules. *Bull. Chem. Soc. Jpn.* **1956**, *29*, 465–470. [[CrossRef](#)]

Disclaimer/Publisher's Note: The statements, opinions and data contained in all publications are solely those of the individual author(s) and contributor(s) and not of MDPI and/or the editor(s). MDPI and/or the editor(s) disclaim responsibility for any injury to people or property resulting from any ideas, methods, instructions or products referred to in the content.